Journal of Sound and Vibration (2000) **233**(5), 775–796
doi:10.1006/jsvi.1999.2735, available online at http://www.idealibrary.com on IDEAL®

VIBRATION ANALYSIS OF TWO BUILDINGS LINKED BY MAXWELL MODEL-DEFINED FLUID DAMPERS

W. S. Zhang and Y. L. Xu

Department of Civil and Structural Engineering, The Hong Kong Polytechnic University, Hung Hom, Kowloon, Hong Kong

(*Received* 15 *June* 1999, *and in final form* 7 *October* 1999)

Fluid dampers that operate on the principle of fluid flow through orifices specially shaped and defined by the Maxwell model have found more and more applications in vibration mitigation of buildings and structures. This paper thus presents an accurate and effective procedure for determining dynamic characteristics and seismic response of adjacent buildings linked by fluid dampers. Dynamic characteristics of damper-linked adjacent buildings are obtained by solving the eigenvalue problem for real non-symmetric matrices. Random seismic response of adjacent buildings linked by dampers is determined by a combination of the state-space method and the pseudo-excitation method. Based on a derived formula, a computer program is written and extensive parametric studies are performed to assess the effectiveness of the fluid damper and to identify beneficial damper relaxation time and damping coefficient at zero frequency. It is shown that using the Maxwell model-defined fluid dampers of proper parameters to link adjacent buildings can increase the modal damping ratios and reduce the seismic responses of adjacent buildings significantly. It is also shown that the behaviour of the adjacent buildings linked by the Maxwell model-defined fluid dampers could be the same as that connected by the Voigt model-defined viscoelastic dampers.

1. INTRODUCTION

Buildings in a modern city are often built close to one another but, in most cases, they are separated without any structural connections or are connected only at the ground level. Hence, earthquake-resistant capacity of each building mainly depends on the building itself. To improve the earthquake resistance of these buildings, the concept of using control devices to link adjacent buildings has been presented.

Kobori *et al.* developed bell-shaped hollow connectors to link very closely spaced adjacent buildings in a complex [1]. Seto and Matsumoto suggested using active actuators to connect a group of buildings for controlling their seismic response [2]. Yamada *et al.* let active actuators generate negative stiffness so as to shift the natural frequencies of adjacent buildings away from the dominant frequency of ground motion to reduce seismic response [3]. Xu *et al.* carried out a preliminary investigation on earthquake-resistance performance of adjacent buildings connected by viscoelastic dampers [4]. In their study, the Voigt model was used to represent viscoelastic dampers, and the seismic response of adjacent buildings was determined by the pseudo-excitation method. The studies demonstrated that viscoelastic dampers of proper parameters could significantly reduce the seismic response of adjacent buildings.

The Voigt model, however, may not be suitable for defining the fluid dampers that utilize fluid flow through specially shaped orifices. Investigations carried out by Constantinou and

0022-460X/00/250775 + 22 $35.00/0

Symans [5] show that the fluid damper exhibits viscoelastic fluid behavior, and that the simplest model to account for this behavior is the Maxwell model. This paper thus aims to present an accurate and effective procedure for determining dynamic characteristics and seismic response of adjacent buildings linked by fluid dampers and to identify beneficial parameters of fluid dampers for achieving the maximum modal damping ratio and the maximum seismic response reduction of adjacent buildings. The effectiveness of the Maxwell model-defined fluid dampers is also compared with the Voigt model-defined viscoelastic dampers.

2. EQUATIONS OF MOTION

To capture important characteristics and seismic behavior of fluid damper-connected adjacent buildings and to make the problem manageable, only the two-dimensional system consisting of two linear elastic shear buildings connected by fluid dampers at each floor of the same level is considered in the present study (see Figure 1). The mass of each building is concentrated at its floor and the stiffness is provided by its massless columns. Both buildings are assumed to be subjected to the same base acceleration, and any effects due to spatial variations of the ground motion or due to soil–structure interactions are neglected. The fluid damper commercially available consists of a cylinder and a stainless-steel piston with a bronze orifice head and an accumulator. The orifice utilizes a series of specially shaped passages to alter flow characteristics with fluid speed. The research carried out by Constantinou and Symans [5] on the fluid damper showed that the Maxwell model proposed by Bird [6] can be used to describe the viscoelastic fluid behavior of the fluid damper applicable to civil engineering structures.

$$f_\Gamma + \lambda \frac{\mathrm{d}f_\Gamma(t)}{\mathrm{d}t} = C_0 \dot{x}, \tag{1}$$

where f_Γ is the damper force, λ is the relaxation time, C_0 is the damping coefficient at zero frequency, and $\dot{x}$ is the damper velocity. The relaxation time λ can be approximately regarded as a ratio of the damping coefficient at zero frequency to the spring stiffness coefficient in a damper system in which one spring and one dashpot are connected in series. However, for a real fluid damper, the relaxation time and the damping coefficient at zero frequency are identified in a slightly different way [5].

Assume that the total of degrees of freedom of two adjacent buildings is N (see Figure 1), in which the number of degrees of freedom of the left building is L with its first floor designated as the first degree of freedom. $N - L$ is then the number of degrees of freedom of the right building with its first floor designated as the $L + 1$ degree of freedom. The equations of motion of the building–damper system can then be expressed as

$$\mathbf{M}\ddot{\mathbf{X}}(t) + \mathbf{C}\dot{\mathbf{X}}(t) + \mathbf{K}\mathbf{X}(t) + \mathbf{f}_\Gamma = -\mathbf{M}\mathbf{E}\ddot{X}_g(t) \tag{2}$$

with the Maxwell model

$$\mathbf{f}_\Gamma + \Lambda\dot{\mathbf{f}}_\Gamma = \mathbf{D}\dot{\mathbf{X}}, \tag{3}$$

where $\mathbf{M}$, $\mathbf{C}$, and $\mathbf{K}$ are the mass, damping, and stiffness matrices of the adjacent buildings, respectively, Λ and $\mathbf{D}$ are the relaxation time and zero-frequency damping coefficient matrices, respectively, of the fluid dampers, $\mathbf{X}(t)$ is the vector of relative displacement response with respect to the ground with the left building's displacements in the first

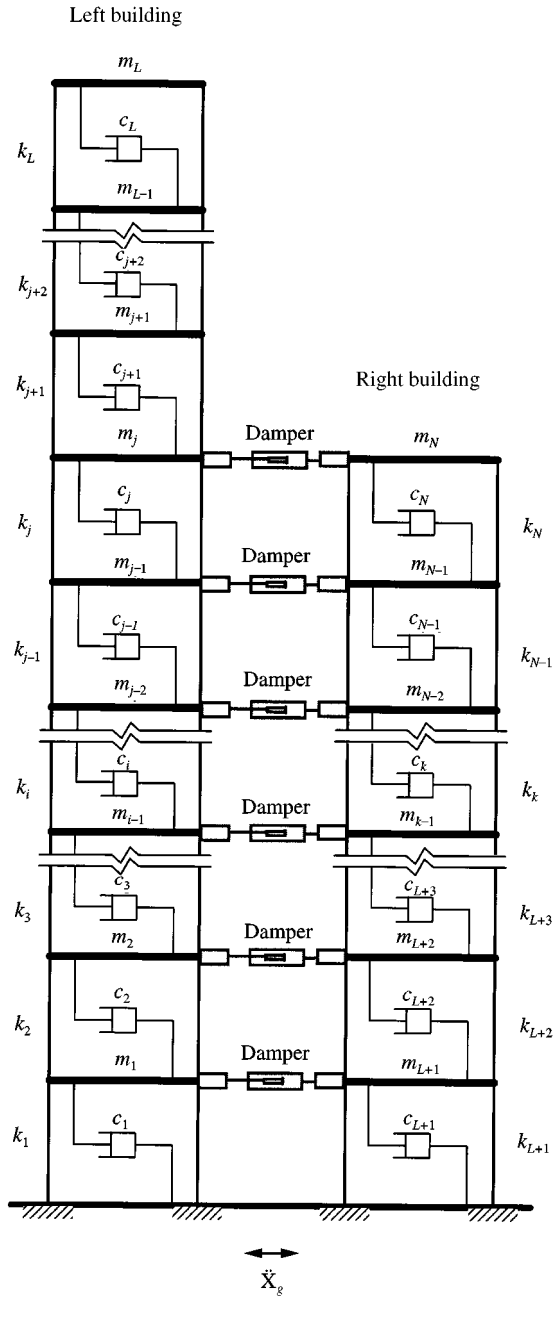

Figure 1. Structural model of adjacent buildings with fluid dampers.

L positions and the right building's displacements in the last $N - L$ positions, $\mathbf{f}_\Gamma$ is the damper force vector, $\mathbf{E}$ is an index vector with all its elements equal to 1, and $\ddot{X}_g(t)$ is the ground acceleration.

Denote the mass, shear stiffness, and external damping coefficient and internal damping coefficient of the adjacent buildings as m_i, k_i, b_i, c_i $(i = 1, 2, \ldots, N)$, respectively, and the

relaxation time and damping coefficient at zero frequency of the fluid damper at the ith floor as λ_i and C_{0i} respectively. The details of each matrix can then be given as follows:

The mass matrix of the adjacent buildings is

$$\mathbf{M} = \mathrm{diag}[m_1, m_2, \ldots, m_N]. \tag{4}$$

The damping matrix of the adjacent building is

$$\mathbf{C} = \mathbf{C}^e + \mathbf{C}^i, \tag{5}$$

in which the external damping matrix is

$$\mathbf{C}^e = \mathrm{diag}[b_1, b_2, \ldots, b_N] \tag{6}$$

and the internal damping matrix is

$$\mathbf{C}^i = \begin{bmatrix} \mathbf{C}_L & \mathbf{0} \\ \mathbf{0} & \mathbf{C}_R \end{bmatrix}, \tag{7}$$

$$\mathbf{C}_L = \begin{bmatrix} c_1 + c_2 & -c_2 & & & & & \\ -c_2 & c_2 + c_3 & -c_3 & & & & \\ & \cdot & & & & & \\ & & \cdot & & & & \\ & & & -c_{L-1} & c_{L-1} + c_L & -c_L & \\ & & & & -c_L & c_L & \end{bmatrix}, \tag{8}$$

$$\mathbf{C}_R = \begin{bmatrix} c_{L+1} + c_{L+2} & -c_{L+2} & & & & & \\ -c_{L+2} & c_{L+2} + c_{L+3} & -c_{L+3} & & & & \\ & \cdot & & & & & \\ & & \cdot & & & & \\ & & & -c_{N-1} & c_{N-1} + c_N & -c_N & \\ & & & & -c_N & c_N & \end{bmatrix}. \tag{9}$$

The stiffness matrix of the adjacent buildings is

$$\mathbf{K} = \begin{bmatrix} \mathbf{K}_L & \mathbf{0} \\ \mathbf{0} & \mathbf{K}_R \end{bmatrix}, \tag{10}$$

$$\mathbf{K}_L = \begin{bmatrix} k_1 + k_2 & -k_2 & & & & & \\ -k_2 & k_2 + k_3 & -k_3 & & & & \\ & \cdot & & & & & \\ & & \cdot & & & & \\ & & & -k_{L-1} & k_{L-1} + k_L & -k_L & \\ & & & & -k_L & k_L & \end{bmatrix}, \tag{11}$$

$$\mathbf{K}_R = \begin{bmatrix} k_{L+1}+k_{L+2} & -k_{L+2} & & & & & \\ -k_{L+2} & k_{L+2}+k_{L+3} & -k_{L+3} & & & & \\ & \cdot & & & & & \\ & & & \cdot & & & \\ & & & & -k_{N-1} & k_{N-1}+k_N & -k_N \\ & & & & & -k_N & k_N \end{bmatrix}. \tag{12}$$

The relaxation time matrix of the fluid damper is

$$\Lambda = \mathrm{diag}[\Lambda_{(N-L)\times(N-L)}, \mathbf{0}_{(2L-N)\times(2L-N)}, \Lambda_{(N-L)\times(N-L)}] \quad (\text{if } N < 2L), \tag{13}$$

in which

$$\Lambda_{(N-L)\times(N-L)} = \mathrm{diag}[\lambda_1, \lambda_2, \ldots, \lambda_{(N-L)}] \tag{14}$$

or

$$\Lambda = \mathrm{diag}[\Lambda_{L\times L}, \Lambda_{L\times L}, \mathbf{0}_{(N-2L)\times(N-2L)}] \quad (\text{if } N \geqslant 2L), \tag{15}$$

$$\Lambda_{L\times L} = \mathrm{diag}[\lambda_1, \lambda_2, \ldots, \lambda_L]. \tag{16}$$

The zero-frequency damping coefficient matrix of the fluid damper is

$$\mathbf{D} = \begin{bmatrix} \mathbf{D}_{(N-L)\times(N-L)} & \mathbf{0}_{(N-L)\times(2L-N)} & -\mathbf{D}_{(N-L)\times(N-L)} \\ \mathbf{0}_{(2L-N)\times(N-L)} & \mathbf{0}_{(2L-N)\times(2L-N)} & \mathbf{0}_{(2L-N)\times(N-L)} \\ -\mathbf{D}_{(N-L)\times(N-L)} & \mathbf{0}_{(N-L)\times(2L-N)} & \mathbf{D}_{(N-L)\times(N-L)} \end{bmatrix} \quad (\text{if } N < 2L), \tag{17}$$

in which

$$\mathbf{D}_{(N-L)\times(N-L)} = \mathrm{diag}[C_{0,1}, C_{0,2}, \ldots, C_{0,N-L}] \tag{18}$$

or

$$\mathbf{D} = \begin{bmatrix} \mathbf{D}_{L\times L} & -\mathbf{D}_{L\times L} & \mathbf{0}_{(N-2L)\times L} \\ -\mathbf{D}_{L\times L} & \mathbf{D}_{L\times L} & \mathbf{0}_{(N-2L)\times L} \\ \mathbf{0}_{(N-2L)\times L} & \mathbf{0}_{(N-2L)\times L} & \mathbf{0}_{(N-2L)\times(N-2L)} \end{bmatrix} \quad (\text{if } N \geqslant 2L), \tag{19}$$

in which

$$\mathbf{D}_{L\times L} = \mathrm{diag}[C_{0,1}, C_{0,2}, \ldots, C_{0,L}]. \tag{20}$$

3. DYNAMIC CHARACTERISTICS

Since the adjacent buildings linked by fluid dampers are non-classically damped systems with unsymmetrical property matrices, the general eigenvalue analysis is employed in this study to determine the dynamic characteristics of the system. The equations of motion (equations (2) and (3)) can be replaced by an equivalent first order differential equation of the form

$$\mathbf{A}\dot{\mathbf{Y}} + \mathbf{B}\mathbf{Y} = \mathbf{F}\ddot{X}_g(t), \tag{21}$$

in which

$$\mathbf{A}=\begin{bmatrix}\mathbf{M} & \mathbf{0} & \mathbf{0}\\ \mathbf{0} & \mathbf{I} & \mathbf{0}\\ \mathbf{0} & \mathbf{0} & \Lambda\end{bmatrix},\qquad \mathbf{B}=\begin{bmatrix}\mathbf{C} & \mathbf{K} & \mathbf{I}\\ -\mathbf{I} & \mathbf{0} & \mathbf{0}\\ -\mathbf{D} & \mathbf{0} & \mathbf{I}\end{bmatrix},\qquad \mathbf{F}=\begin{Bmatrix}-\mathbf{ME}\\ \mathbf{0}\\ \mathbf{0}\end{Bmatrix}\quad\text{and}\quad \mathbf{Y}=\begin{Bmatrix}\dot{\mathbf{X}}\\ \mathbf{X}\\ \mathbf{f}_\Gamma\end{Bmatrix} \tag{22}$$

and $\mathbf{I}$ is the identity matrix. Matrices $\mathbf{A}$ and $\mathbf{B}$ are of size $3N\times 3N$.

Since the matrix $\mathbf{B}$ in equation (22) is not symmetric, one needs to solve the following two adjoining eigenvalue problems:

$$(s\mathbf{A}+\mathbf{B})\hat{\phi}=\mathbf{0}\quad\text{and}\quad(s\mathbf{A}^{\mathrm{T}}+\mathbf{B}^{\mathrm{T}})\hat{\psi}=\mathbf{0}, \tag{23}$$

where s is an eigenvalue, and $\hat{\phi}$ and $\hat{\psi}$ are the corresponding right eigenvector and left eigenvector, respectively, of the form

$$\hat{\phi}=\begin{Bmatrix}s\phi\\ \phi\\ \theta\end{Bmatrix},\qquad \hat{\psi}=\begin{Bmatrix}s\psi\\ \psi\\ \vartheta\end{Bmatrix}. \tag{24, 25}$$

The solution of each eigenvalue problem comprises a set of $3N$ eigenvalues and eigenvectors that are either real or exist in complex conjugate pairs. Among these $3N$ eigenvalues and eigenvectors, there are N real eigenvalues and eigenvectors attributed to fluid dampers. If the practical damper parameters are taken into consideration, the N real eigenvalues attributed to fluid dampers are very large in general. Some of them may be infinite if the damper relaxation time is equal to zero or there is no fluid damper at all. For this reason, the N real eigenvalues related to the fluid dampers are denoted by s_{j+2N} ($j=1, 2, \ldots, N$) in this study.

If the adjacent buildings linked by fluid dampers still belong to an underdamped system, the remaining $2N$ eigenvalues and eigenvectors (either right eigenvectors or left eigenvectors) will be in complex conjugate pairs.

$$\hat{\phi}_j=\hat{\phi}^*_{j+N}\quad\text{and}\quad s_j=s^*_{j+N}. \tag{26}$$

Each eigenvalue can be written in the form

$$s_j=s^*_{j+N}=-\omega_i\xi_j+\mathrm{i}\omega_{dj}\quad(j=1, 2, \ldots, N), \tag{27}$$

in which

$$\omega_j=|s_j|,\quad \xi_j=-\mathrm{Re}(s_j)/|s_j|\quad\text{and}\quad \omega_{dj}=\omega_j\sqrt{1-\xi_j^2}. \tag{28}$$

ω_j, ω_{dj}, and ξ_j are the modal frequency, the damped modal frequency, and the modal damping ratio, respectively, associated with mode j. The superscript * means the conjugation. For the underdamped mode, the value of ξ_j is always less than one.

In some cases, which depend on the selected damper parameters, there are some real-valued negative pairs among the $2N$ eigenvalues. The system may be called the mixed damped system in this situation, and it is convenient to express real pair s_j in the following form analogous to equation (27):

$$s_j=-\omega_j\xi_j+\omega_{dj}\quad(j=1, 2, \ldots, N), \tag{29}$$

$$s_{j+N}=-\omega_j\xi_j-\omega_{dj}\quad(j=1, 2, \ldots, N), \tag{30}$$

in which ω_j, ω_{dj} and ξ_j are determined, respectively, by

$$\omega_j = \sqrt{s_j s_{j+N}}, \qquad \xi_j = -(s_j + s_{j+N})/(2\omega_j)$$
$$\text{and} \quad \omega_{dj} = \omega_j \sqrt{\xi_j^2 - 1} = (s_j - s_{j+N})/2. \tag{31}$$

The value of ξ_j is now equal to or greater than one.

The eigenvalue analysis of a fluid damper-adjacent building system carried out here is mainly to determine the modal damping ratio and natural frequency of the system attributed to fluid dampers and to find optimal damper parameters for achieving the maximum modal damping ratio. Thus, it is desirable to know the sensitivities of the jth modal damping ratio and jth natural frequency to the mth damper relaxation time or the mth damper damping coefficient at zero frequency. For this purpose, the partial derivative of the first expression in equation (23) with respect to the mth damper relaxation time λ_m is taken, which leads to

$$\left(\frac{\partial s_j}{\partial \lambda_m}\mathbf{A} + s_j \frac{\partial \mathbf{A}}{\partial \lambda_m}\right)\hat{\phi}_j + (s_j\mathbf{A} + \mathbf{B})\frac{\partial \hat{\phi}_j}{\partial \lambda_m} = \mathbf{0}. \tag{32}$$

Multiplying equation (32) by $\hat{\psi}_j^{\mathrm{T}}$ and using the relationship

$$\hat{\psi}_j^{\mathrm{T}}(s_j\mathbf{A} + \mathbf{B}) = \mathbf{0}, \tag{33}$$

one obtains

$$\frac{\partial s_j}{\partial \lambda_m} = -\left(s_j \hat{\psi}_j^{\mathrm{T}} \frac{\partial \mathbf{A}}{\partial \lambda_m}\hat{\phi}_j\right) \Big/ A_j = -s_j \Lambda_{jm}/A_j, \tag{34}$$

in which

$$\Lambda_{jm} = \vartheta_j^{\mathrm{T}} \frac{\partial \Lambda}{\partial \lambda_m}\theta_j, \tag{35}$$

$$A_j = \hat{\psi}_j^{\mathrm{T}}\mathbf{A}\hat{\phi}_j. \tag{36}$$

For the underdamped mode, differentiating the following relationships with respect to the mth damper relaxation time λ_m:

$$s_j s_j^* = \omega_j^2 \quad \text{and} \quad s_j + s_j^* = -2\xi_j\omega_j \tag{37}$$

and using equation (34) yields

$$\frac{\partial \omega_j}{\partial \lambda_m} = -\omega_j \mathrm{Re}\left(\frac{\Lambda_{jm}}{A_j}\right), \tag{38}$$

$$\frac{\partial \xi_j}{\partial \lambda_m} = -\sqrt{1 - \xi_j^2}\,\mathrm{Im}\left(\frac{\Lambda_{jm}}{A_j}\right). \tag{39}$$

These two equations can be used for the sensitivity study of the natural frequency and modal damping ratio with respect to damper relaxation time.

In a similar way, one can obtain

$$\frac{\partial s_j}{\partial C_{0,m}} = -\left(\hat{\psi}_j^{\mathrm{T}} \frac{\partial \mathbf{B}}{\partial C_{0,m}}\hat{\phi}_j\right)/A_j = -s_j D_{jm}/A_j, \tag{40}$$

in which

$$D_{jm} = \vartheta_j^{\mathrm{T}} \frac{\partial \mathbf{D}}{\partial C_{0,m}}\phi_j. \tag{41}$$

For the underdamped mode, the sensitivities of the natural frequency and modal damping ratio with respect to zero-frequency damping coefficient $C_{0,m}$ are as follows:

$$\frac{\partial \omega_j}{\partial C_{0,m}} = \omega_j \mathrm{Re}\left(\frac{D_{jm}}{A_j}\right), \tag{42}$$

$$\frac{\partial \xi_j}{\partial C_{0,m}} = \sqrt{1-\xi_j^2}\,\mathrm{Im}\left(\frac{D_{jm}}{A_j}\right). \tag{43}$$

For the overdamped mode, one can get the following four equations for sensitivity study:

$$\frac{\partial \omega_j}{\partial \lambda_m} = -\frac{\omega_j}{2}\left(\frac{\Lambda_{jm}}{A_{jm}} + \frac{\Lambda_{j+N,m}}{A_{j+N,m}}\right), \tag{44}$$

$$\frac{\partial \xi_j}{\partial \lambda_m} = \frac{\sqrt{\xi_j^2-1}}{2}\left(\frac{\Lambda_{jm}}{A_{jm}} - \frac{\Lambda_{j+N,m}}{A_{j+N,m}}\right), \tag{45}$$

$$\frac{\partial \omega_j}{\partial \lambda_m} = \frac{\omega_j}{2}\left(\frac{D_{jm}}{A_{jm}} + \frac{D_{j+N,m}}{A_{j+N,m}}\right), \tag{46}$$

$$\frac{\partial \xi_j}{\partial \lambda_m} = -\frac{\sqrt{\xi_j^2-1}}{2}\left(\frac{D_{jm}}{A_{jm}} - \frac{D_{j+N,m}}{A_{j+N,m}}\right). \tag{47}$$

4. SEISMIC RESPONSE

The state-space method adopts the following co-ordinate transformation to decouple equation (21).

$$\mathbf{Y} = \Phi \mathbf{Z}, \tag{48}$$

where $\mathbf{Z}$ is the $3N$-dimensional generalized co-ordinate vector and Φ is the $3N \times 3N$ complex modal matrix.

$$\Phi = [\hat{\phi}_1, \hat{\phi}_2, \ldots, \hat{\phi}_{3N}]. \tag{49}$$

By using the co-ordinate transformation and the orthogonality between the right eigenvectors and the left eigenvectors, equation (21) can be reduced to $3N$ decoupled modal equations with the jth modal equation being

$$\dot{Z}_j - s_j Z_j = r_j \ddot{X}_g(t), \tag{50}$$

in which

$$r_j = \hat{\psi}_j^{\mathrm{T}} \mathbf{F}/A_j = -s_j \psi_j^{\mathrm{T}} \mathbf{M}\mathbf{E}/A_j. \tag{51}$$

Assume that the ground acceleration $\ddot{X}_g(t)$ is a stationary random process and its power spectral density function is given as $S_g(\omega)$. A pseudo-excitation method in conjuncation with the state-space method can be developed to determine the seismic response of adjacent buildings linked by fluid dampers. Pseudo-excitation is constituted for a given frequency ω as

$$\ddot{X}_g(t) = \sqrt{S_g(\omega)}\,\mathrm{e}^{\mathrm{i}\omega t}. \tag{52}$$

The solution of the first order equation (50) to the pseudo-excitation is

$$Z_j(\omega, t) = \frac{r_j}{\mathrm{i}\omega - s_j}\sqrt{S_g(\omega)}\,\mathrm{e}^{\mathrm{i}\omega t} \quad (j = 1, 2, \ldots, 3N). \tag{53}$$

Substituting equation (53) into equation (48) and comparing with the last expression of equation (22), one obtains

$$\mathbf{X}(\omega, t) = \sum_{j=1}^{3N} \phi_j Z_j(\omega, t) = \sum_{j=1}^{3N} \phi_j \frac{r_j}{\mathrm{i}\omega - s_j} \sqrt{S_g(\omega)} \mathrm{e}^{\mathrm{i}\omega t}. \tag{54}$$

Since the eigenvectors are in pairs for either the underdamped or the overdamped mode, equation (54) can be reduced to

$$\mathbf{X}(\omega, t) = \left(\sum_{j=1}^{N} H_j(\omega)(\mathrm{i}\omega\alpha_j + \beta_j) + \sum_{j=2N+1}^{3N} \phi_j \frac{r_j}{\mathrm{i}\omega - s_j} \right) \sqrt{S_g(\omega)} \mathrm{e}^{\mathrm{i}\omega t} = \mathbf{X}(\omega) \mathrm{e}^{\mathrm{i}\omega t}, \tag{55}$$

in which $\mathbf{X}(\omega)$ is called the pseudo-displacement, and $H_j(\omega)$ is the frequency response function for the jth mode. When the jth mode is an underdamped mode

$$\alpha_j = 2\,\mathrm{Re}(\phi_j r_j) \quad \text{and} \quad \beta_j = -2\,\mathrm{Re}(\phi_j r_j s_j^*). \tag{56}$$

When the jth mode is an overdamped mode

$$\alpha_j = (\phi_j r_j + \phi_{j+N} r_{j+N}) \quad \text{and} \quad \beta_j = -(\phi_j r_j s_{j+N} + \phi_{j+N} r_{j+N} s_j). \tag{57}$$

In a similar way, the pseudo-velocity response can be obtained by

$$\dot{\mathbf{X}}(\omega) = \left(\sum_{j=1}^{N} H_j(\omega)(\mathrm{i}\omega\mu_j + \nu_j) + \sum_{j=2N+1}^{3N} s_j \phi_j \frac{r_j}{\mathrm{i}\omega - s_j} \right) \sqrt{S_g(\omega)}. \tag{58}$$

When the jth mode is an underdamped mode,

$$\mu_j = 2\mathrm{Re}(s_j \phi_j r_j) \quad \text{and} \quad \nu_j = -2\omega_j^2\,\mathrm{Re}(\phi_j r_j). \tag{59}$$

When the jth mode is an overdamped mode,

$$\mu_j = (s_j \phi_j r_j + s_{j+N} \phi_{j+N} r_{j+N}) \quad \text{and} \quad \nu_j = -\omega_j^2 (\phi_j r_j + \phi_{j+N} r_{j+N}). \tag{60}$$

In practice, only the first q ($q \ll 3N$) modes are needed to be included when calculating seismic response. Thus, the pseudo-displacement can be simplified as

$$\mathbf{X}(\omega) = \left(\sum_{j=1}^{q} H_j(\omega)(\mathrm{i}\omega\alpha_j + \beta_j) \right) \sqrt{S_g(\omega)}. \tag{61}$$

Once the pseudo-displacement is determined, the pseudo-internal force can be easily determined following a static analysis. For instance, the pseudo-shear force of the adjacent buildings can be calculated by

$$\mathbf{Q}(\omega, t) = \mathbf{G}\mathbf{X}(\omega, t), \tag{62}$$

where

$$\mathbf{G} = \begin{bmatrix} \mathbf{G}_L & 0 \\ 0 & \mathbf{G}_R \end{bmatrix} \tag{63}$$

and

$$\mathbf{G}_L = \begin{bmatrix} k_1 & & & & & \\ -k_2 & k_2 & & & & \\ & \ddots & & & & \\ & & \ddots & & & \\ & & & -k_{L-1} & k_{L-1} & \\ & & & & -k_L & k_L \end{bmatrix}, \tag{64}$$

$$\mathbf{G}_R = \begin{bmatrix} k_{L+1} & & & & & \\ -k_{L+2} & k_{L+2} & & & & \\ & \ddots & & & & \\ & & \ddots & & & \\ & & & -k_{N-1} & k_{N-1} & \\ & & & & -k_N & k_N \end{bmatrix}. \tag{65}$$

The response spectral matrix can be obtained as

$$\mathbf{S}_{XX}(\omega) = \mathbf{X}^*(\omega)\mathbf{X}^{\mathrm{T}}(\omega), \tag{66}$$

$$\mathbf{S}_{\dot{X}\dot{X}}(\omega) = \dot{\mathbf{X}}^*(\omega)\dot{\mathbf{X}}^{\mathrm{T}}(\omega), \tag{67}$$

$$\mathbf{S}_{QQ}(\omega) = \mathbf{Q}^*(\omega)\mathbf{Q}^{\mathrm{T}}(\omega). \tag{68}$$

It should be pointed out that the pseudo-excitation method used in conjunction with the state-space method is a natural extension of the original pseudo-excitation method suggested by Lin *et al.* for the classically damped structures (or uncontrolled structures) [7]. By using the mixed method proposed here, the cross-correlation terms between vibration modes in the seismic response can be retained for the non-classically damped systems. The present mixed method can also easily provide internal force and damper force responses. Finally, the standard deviation displacement and acceleration responses of the jth floor can be evaluated as

$$\sigma_{X_j}^2 = \int_{-\infty}^{+\infty} S_{X_jX_j}(\omega)\,\mathrm{d}\omega, \qquad \sigma_{\dot{X}_j}^2 = \int_{-\infty}^{+\infty} \omega^2 S_{X_j\dot{X}_j}(\omega)\,\mathrm{d}\omega. \tag{69}$$

5. APPLICATION

For application, two 20-story buildings having the same floor elevations with dampers connecting two neighboring floors are used. The mass, shear stiffness, and external damping coefficient of the left building (also called the stiffer building, see Figure 1) are uniform for all stories with a mass of $1{\cdot}29 \times 10^6$ kg, a shear stiffness of $4{\cdot}0 \times 10^9$ N/m, and an external damping coefficient of $1{\cdot}0 \times 10^5$ Ns/m. For the right building (also called the softer building), the mass, shear stiffness, and external damping coefficient are uniform for all stories with the same mass and damping coefficient as the left building except the shear stiffness which is $2{\cdot}0 \times 10^9$ N/m only. Hence, the two buildings have the same height but the right building is most slender than the left building. The internal damping coefficients are set to zero for both the buildings. The same adjacent buildings were used by Xu *et al.* for the

adjacent buildings linked by Voigt model-defined viscoelastic dampers [4]. Thus, a comparison of the effectiveness between the Voigt model-defined viscoelastic dampers and the Maxwell model defined fluid dampers can be made.

The Kanai–Tajimi filtered white-noise spectrum is used as the ground acceleration spectrum in the computation. The characteristic ground frequency, the characteristic damping ratio, and the intensity of an earthquake in the ground acceleration spectrum are selected as $\omega_g = 15{\cdot}0$ rad/s, $\xi_g = 0{\cdot}65$, and $S_0 = 4{\cdot}65 \times 10^{-4}\,\mathrm{m^2/rad\,s^3}$ respectively.

$$S_g(\omega) = \frac{1 + 4\xi_g^2(\omega/\omega_g)^2}{[1 - (\omega/\omega_g)^2]^2 + 4\xi_g^2(\omega/\omega_g)^2}\, S_0. \tag{70}$$

Fluid dampers used to connect every two neighboring floors are assumed to have the same relaxation time λ and zero frequency-damping coefficient C_0.

5.1. MODAL FREQUENCIES AND DAMPING RATIOS

Within the frequency range between 0 and 20·00 rad/s, the first three modal frequencies of the right building without fluid dampers are 3·02, 9·03 and 14·99 rad/s. The first two modal frequencies of the left building without fluid dampers are 4·27 and 12·77 rad/s. When every two neighboring floors of the adjacent buildings are linked by the fluid dampers of the same relaxation time of 0·001 s and the same zero frequency damping coefficient of $1{\cdot}42 \times 10^6$ N s/m, the first five modal frequencies of the damper–building system obtained from the complex eigenvalue analysis are 3·28, 3·93, 9·11, 12·68 and 15·04 rad/s. Obviously, using the fluid dampers to link the adjacent buildings slightly changes the first modal frequency of each building but other natural frequencies remain almost unchanged. The retention of the natural frequencies of the unlinked buildings after the installation of the joint dampers is especially desirable for the adjacent buildings that have been already built and need to be strengthened.

As to modal damping ratios, the first three modal damping ratios in the unlinked left building are calculated as 1·28, 0·43, and 0·26% respectively. The first two model damping ratios in the unlinked right building are computed as 0·91 and 0·30%. For the linked building–damper system, the first five modal damping ratios obtained from the complex eigenvalue analysis are 22·27, 11·47, 6·56, 4·60, and 3·93%. Thus, one can expect that the seismic response of the adjacent buildings will be tremendously reduced.

The first five natural frequencies and modal damping ratios of the adjacent buildings linked by the Voigt model-defined viscoelastic dampers were also calculated by the writers. With the optimal damper stiffness of $1{\cdot}0 \times 10^5$ N/m and optimal damper damping coefficient of $1{\cdot}0 \times 10^6$ N s/m, the first five modal frequencies of the damper–building system are 3·14, 4·12, 0·97, 12·73 and 15·02 rad/s. The first five modal damping ratios of the system are 14·44, 9·68, 4·73, 3·33, and 2·85%. Clearly, the use of fluid dampers provides more damping ratios than the use of viscoelastic dampers. However, the first two natural frequencies of the damper–building system with either fluid dampers or viscoelastic dampers are far away from the dominant frequency of the ground acceleration (15 rad/s in this study). Thus, the earthquake-response reduction of the damper–building system with the fluid dampers may not be much larger than the system with the viscoelastic dampers.

The relaxation time and zero-frequency damping coefficient of the fluid dampers used in the foregoing calculation are optimal parameters determined through a parametric study. In the parametric study, the modal frequencies and damping ratios of the building–damper system are computed against the relaxation time and zero-frequency damping coefficient of

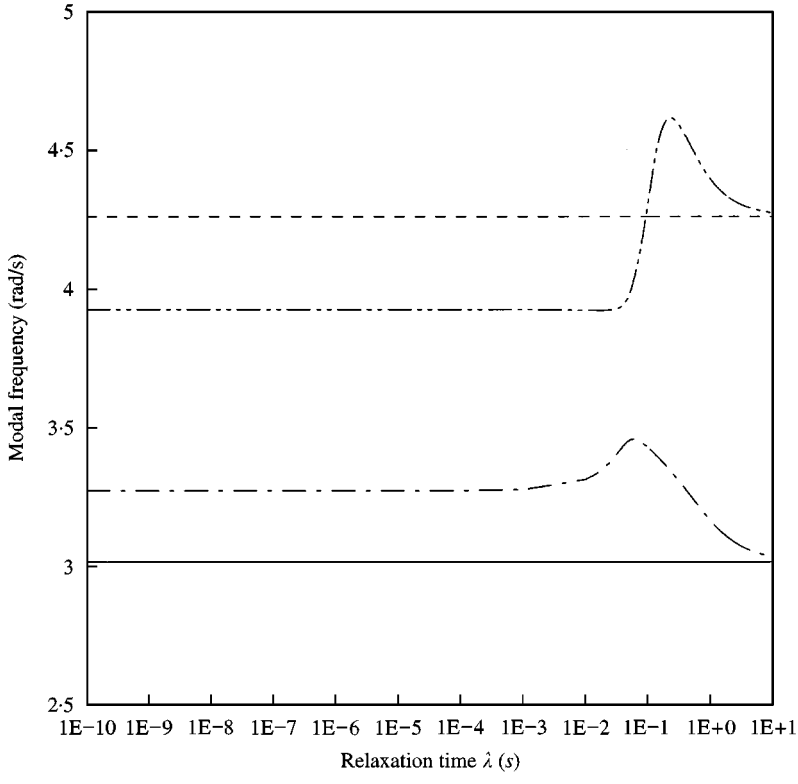

Figure 2. Variations of modal frequencies with relaxation time: ——, ω_1, $C_0 = 10$; – – – –, ω_2, $C_0 = 10$; — · —, ω_1, $C_0 = 1{\cdot}42 \times 10^6$; — · · —, ω_2, $C_0 = 1{\cdot}42 \times 10^6$.

the dampers. The beneficial relaxation time λ and zero-frequency damping coefficient C_0 of the dampers can thus be found for achieving the maximum modal damping ratio and remaining the original modal frequencies almost unchanged. Figure 2 displays variations of the first and second modal frequencies of the system with relaxation time λ for zero-frequency damping coefficient $C_0 = 10$ and $1{\cdot}42 \times 10^6$ N s/m. It is seen that for the very small zero-frequency damping coefficient $C_0 = 10$ N s/m, the modal frequencies are almost independent of relaxation time and the modal frequencies remain the same as those of the unlinked adjacent buildings. This is because the very small zero-frequency damping coefficient plus very small relaxation time indicate that the connections provided by the fluid dampers for the two buildings are very weak. For the zero-frequency damping coefficient $C_0 = 1{\cdot}42 \times 10^6$ N s/m, the modal frequencies are slightly change. The modal frequencies, however, do not depend on relaxation time until the relaxation time is equal to 0·01 s. If the relaxation time is beyond this value, the modal frequencies of the system will first increase rapidly and then decrease rapidly towards those of the unlinked adjacent buildings. This is mainly due to the large zero-frequency damping coefficient and the increase in the relaxation time.

Figure 3 shows variations of the first two modal damping ratios of the system with relaxation time for three zero-frequency damping coefficients. For the very small zero-frequency damping coefficient $C_0 = 10$ N s/m, the first two modal damping ratios are almost the same as those for the unlinked adjacent buildings and do not depend on the relaxation time concerned. With higher zero-frequency damping coefficients, the first two

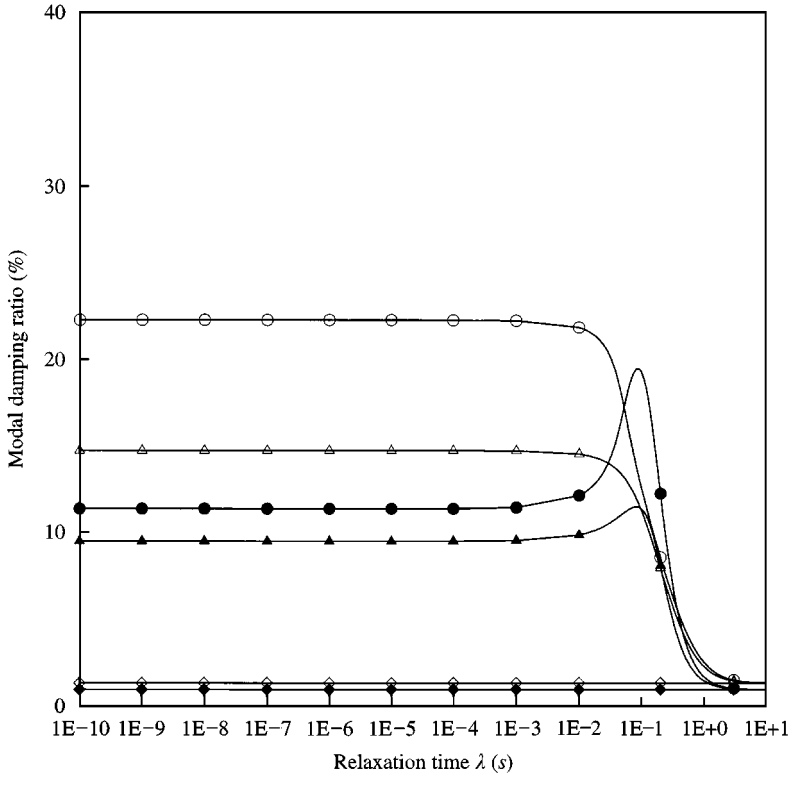

Figure 3. Variations of modal damping ratios with relaxation time: —◇—, ξ_1, $C_0 = 10$; —◆—, ξ_2, $C_0 = 10$; —△—, ξ_1, $C_0 = 10^6$; —▲—, ξ_2, $C_0 = 10^6$; —○—, ξ_1, $C_0 = 1{\cdot}42 \times 10^6$; —●—, ξ_2, $C_0 = 1{\cdot}42 \times 10^6$.

modal damping ratios of the system increase significantly and remain almost constant within a relaxation time ranging from zero to 0·001 s. Beyond this range, the first modal damping ratio will decrease rapidly with the increasing relaxation time and the second modal damping ratio will first increase and then decrease towards those of unlinked adjacent buildings. The reason behind these observations is similar to that for the variation of natural frequencies. Furthermore, although the trend in Figure 3 shows that as the relaxation time is increased to between 0·01 and 0·1 s, the two curves intersect and the modal damping ratio is of approximately 17% for both the first and second modes of vibration; the damping ratio is very sensitive to the small change in relaxation time. Thus, from a practical point of view, the beneficial value of time relaxation is selected as 0·001 s in this study. Figure 3 also indicates that the zero-frequency damping coefficient affects the first two modal damping ratios of the system significantly.

The variations of the first five modal frequencies with zero-frequency damping coefficient are shown in Figure 4 for the relaxation time of 0·001 s. All the modal frequencies remain almost constant when the zero-frequency damping coefficient is less than 5×10^5 N s/m. After that, the three modal frequencies dominated by the softer buildings (ω_1, ω_3, and ω_5) become larger while the two modal frequencies governed by the stiffer building (ω_2 and ω_4) become smaller. This is because for a given relaxation time, the very large zero-frequency ratio damping coefficient is associated with the very large spring stiffness coefficient so that the connections between the two building become more and more strong and the natural frequencies of the two buildings more and more close.

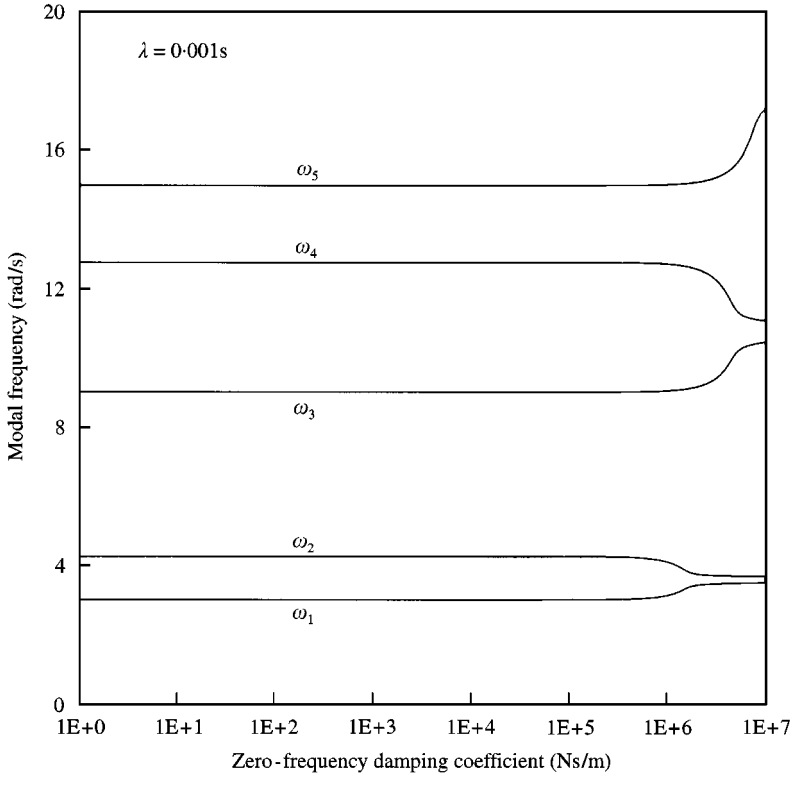

Figure 4. Variations of modal frequencies with zero-frequency damping coefficient.

The modal damping ratios in the three modes dominated by the softer building (ξ_1, ξ_3 and ξ_5) are depicted in Figure 5(a) against the zero-frequency damping coefficient while the modal damping ratios in the two modes dominated by the stiffer building (ξ_2 and ξ_4) are plotted in Figure 5(b). It is seen that for the zero-frequency damping coefficient less than about 1×10^4 N s/m, the dampers have no effect on the modal damping ratios, and the modal damping ratios come mainly from the buildings themselves. As the zero-frequency damping coefficient increases, all the modal damping ratios increase. However, when the damper zero-frequency damping coefficient is increased to certain values, the modal damping ratios dominated by the stiffer building decrease while the modal damping ratios governed by the softer building increase further and soon these modes of the softer building become overdamped modes. Therefore, for a very large zero-frequency damping coefficient, the system behaves like a lightly damped stiffer building supported by a softer building that has almost no vibration due to very high vibration energy dissipation capability. As for the adjacent buildings concerned, the beneficial value of zero-frequency damping coefficient should be selected as $1{\cdot}42 \times 10^6$ N s/m so that the second mode of the system (the first mode of the stiffer building) will have the maximum value of ξ_2. Of course, the first two modal frequencies of the system have thus a slight change as seen from Figure 4.

Compared with the adjacent buildings linked by the Voigt model-defined viscoelastic damper, it is found that the variations of modal damping ratio and modal frequency with respect to the zero-frequency damping coefficient of fluid damper are almost the same as those with respect to the damping coefficient of viscoelastic damper. The variations of modal damping ratio and modal frequency with respect to the relaxation time of fluid

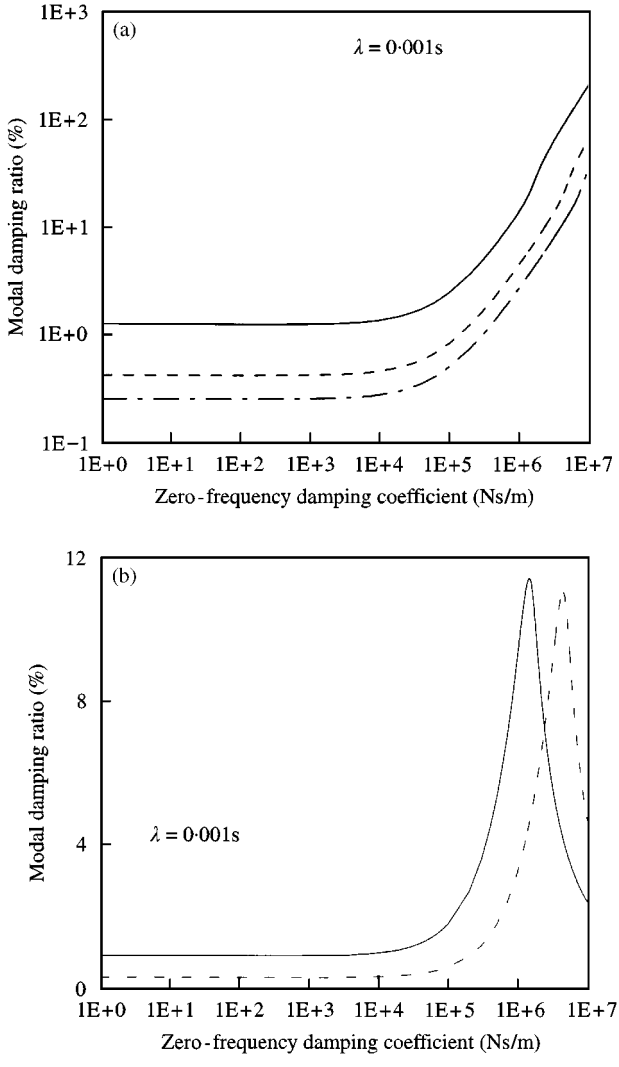

Figure 5. Variations of modal damping ratios with zero-frequency damping coefficient. (a) Modal damping ratios in right building: ——, ξ_1; – – – –, ξ_3; —·—, ξ_5; (b) Modal damping ratios in left building: ——, ξ_2, – – –, ξ_4.

damper are almost the same as those with respect to the stiffness of the viscoelastic damper when the relaxation time of fluid damper is less than 0·001 s and the stiffness of viscoelastic damper is less than $1{\cdot}0 \times 10^5$ N/m. However, when the relaxation time of the fluid damper is much larger than 0·001 s and the stiffness of the viscoelastic damper is much larger than $1{\cdot}0 \times 10^5$ N/m, the variations of modal frequency in the two cases are different: the adjacent buildings tend to be rigidly connected in the case of the viscoelastic dampers but tend to be completely separated in the case of the fluid dampers.

A sensitivity study of modal frequency and modal damping ratio to relaxation time and zero-frequency damping coefficient is carried out at the optimum values C_0 of $1{\cdot}42 \times 10^6$ Ns/m and λ of 0·001 s. The sensitivity of the first modal frequency ω_1 to changes in λ_i or C_{0i} ($i = 1, 2, \ldots, 20$) is depicted in Figure 6(a) in terms of $\partial\omega_1/\partial\lambda_i$ and $\partial\omega_1/\partial C_{0i}$. The sensitivity of the first-modal damping ratio ξ_1 to changes in λ_i or C_{0i} ($i = 1, 2, \ldots, 20$) is

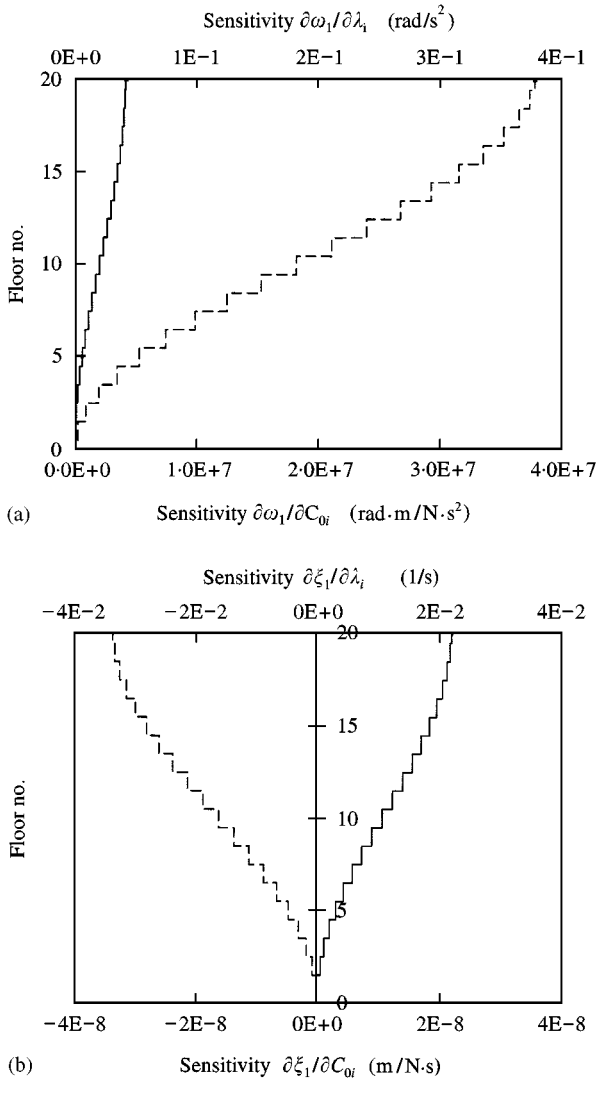

Figure 6. Sensitivities of modal frequency and modal damping ratio. (a) Sensitivity of modal frequency: ——, to C_{0i}; – – –, to λ_i; (b) Sensitivity of modal damping ratio: ——, to C_{0i}, – – –, to λ_i.

plotted in Figure 6(b) by means of $\partial\xi_1/\partial\lambda_i$ and $\partial\xi_1/\partial C_{0i}$. As expected, the first modal frequency and first modal damping ratio are more sensitive to the damper at the top of the buildings than others. The very low sensitivity to the dampers near the bottom of the buildings may indicate no need to install these dampers. The negative sensitivity, or gradient, of the first modal damping ratio to relaxation time is because as the relaxation time increases, the first modal damping ratio decreases. Similar sensitivity results are found for the second modal frequency and damping ratio. Since all the sensitivity values are small even for the damper at the top of the buildings, one may conclude that the small deviations of the dampers from its optimal values ($C_0 = 1{\cdot}42 \times 10^6$ N s/m and $\lambda = 0{\cdot}001$ s) may not affect the control efficiency.

5.2. SEISMIC RESPONSE

A seismic response analysis is carried out to investigate variations in seismic response of the adjacent buildings with damper parameters to see if the optimal damper parameters identified from the modal analysis are the same as those from the seismic response analysis under the given earthquake-excitation spectrum. Then, the effectiveness of the dampers of optimal parameters in seismic response mitigation is examined. Because of the limitation of space, only a few typical figures are given in this paper.

Figure 7(a) and 7(b) depict the variations of the top-floor displacement responses of the left building and the right building, respectively, with relaxation time for several zero-frequency damping coefficients. It is seen that the top-floor displacement responses of

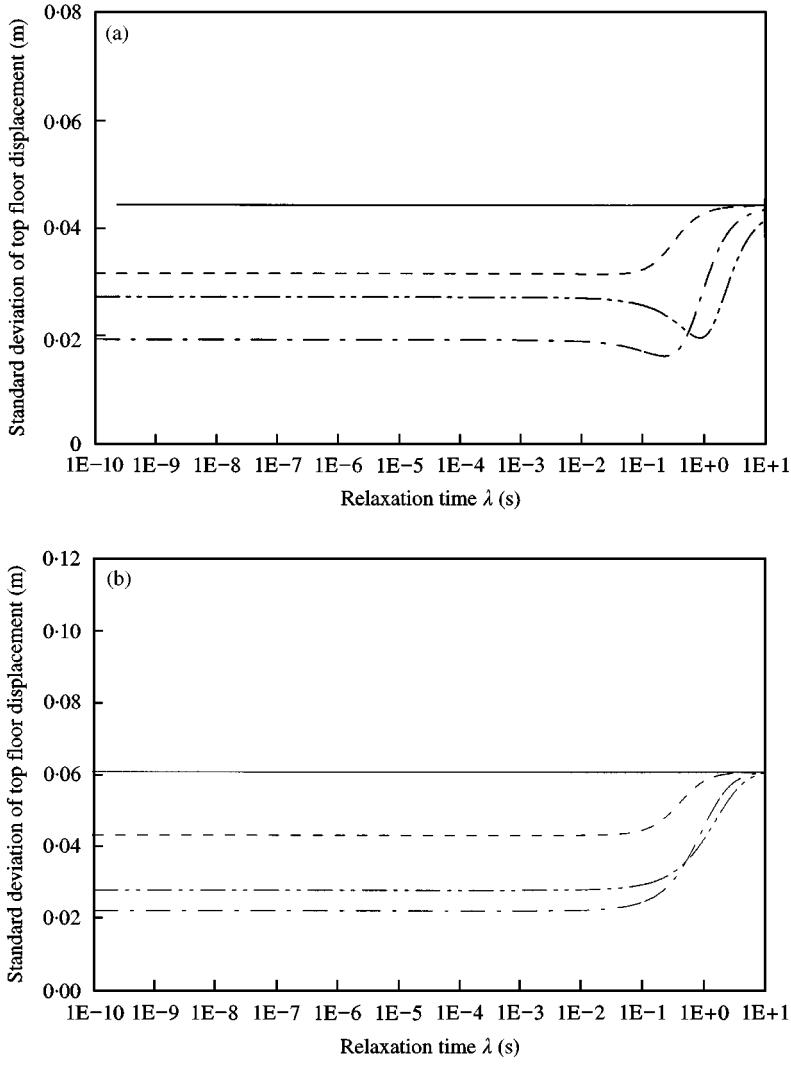

Figure 7. Top-floor displacement response of adjacent buildings versus relaxation time. (a) Left building: ——, $C_0 = 10$(N s/m); – – – –, $C_0 = 10^5$(N s/m); —·—, $C_0 = 1{\cdot}42 \times 10^6$(N s/m); —··—, $C_0 = 5 \times 10^6$(N s/m); (b) Right building ——, $C_0 = 10$(N s/m); – – – –, $C_0 = 10^5$(N s/m); —·—, $C_0 = 1{\cdot}42 \times 10^6$(N s/m); —··—, $C_0 = 5 \times 10^6$(N s/m).

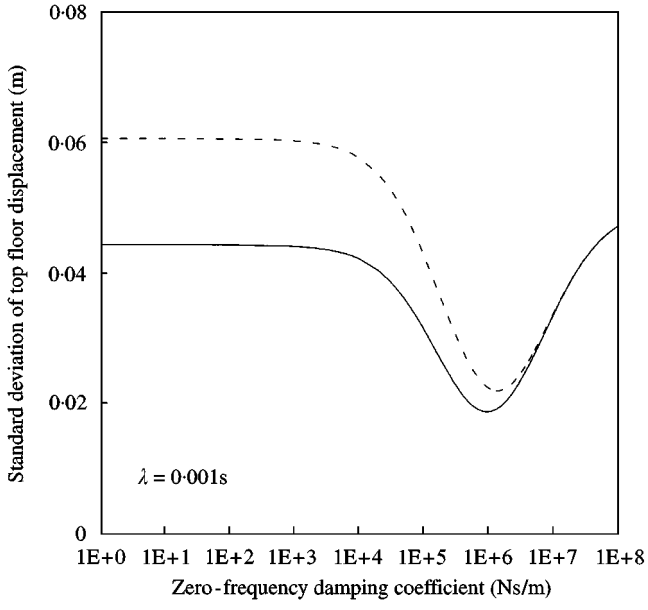

Figure 8. Top-floor displacement response of adjacent buildings versus zero-frequency damping coefficient: ——, Left building; – – –, Right building.

both the left and right buildings are not affected by relaxation time if the relaxation time is less than 0·001 s. The fact that the response mitigation is not sensitive to relaxation time within a certain range is very helpful for the practical application of fluid dampers. The further increase in the relaxation time for 0·001 s may reduce the seismic response of the left building, but it certainly increases the seismic response of the right building. In particular, when the relaxation time reaches a value above 10 s, the two buildings behave almost as though they are not connected. As a result, no matter what values the zero-frequency damping coefficient one, the damper totally loses its effectiveness. It is clear from the foregoing two figures that to achieve the maximum reduction of the dynamic response of both buildings, the optimum relaxation time should be less than 0·001 s, which is the same as the one found from the modal analysis. In addition, it can be seen from Figure 7(a) and 7(b) that there is an optimal zero-frequency damping coefficient between 10^5 and 5×10^6 N s/m.

To find the optimal zero-frequency damping coefficient, the seismic responses including the top-floor displacement response, the base shear force response, and the top-floor acceleration response of both buildings are computed over a wide range of zero-frequency damping coefficient with the optimum relaxation time being 0·001 s. Figure 8 shows the variations of the top-floor displacement responses of the two buildings with zero-frequency damping coefficient. It is seen that the optimum zero-frequency damping coefficient is $0{\cdot}98 \times 10^6$ N s/m for the left building or $1{\cdot}42 \times 10^6$ N s/m for the right building. The value $1{\cdot}42 \times 10^6$ N s/m is the same as the one found from the modal analysis. With the decrease in the zero-frequency damping coefficient from the optimum value, the performance of the damper deteriorates gradually and as the zero-frequency damping coefficient approaches zero, the two buildings finally return to the unlinked situation. On the other hand, if the zero-frequency damping coefficient increases from the optimum value, the performance of the damper also declines and as the zero-frequency damping coefficient becomes very large

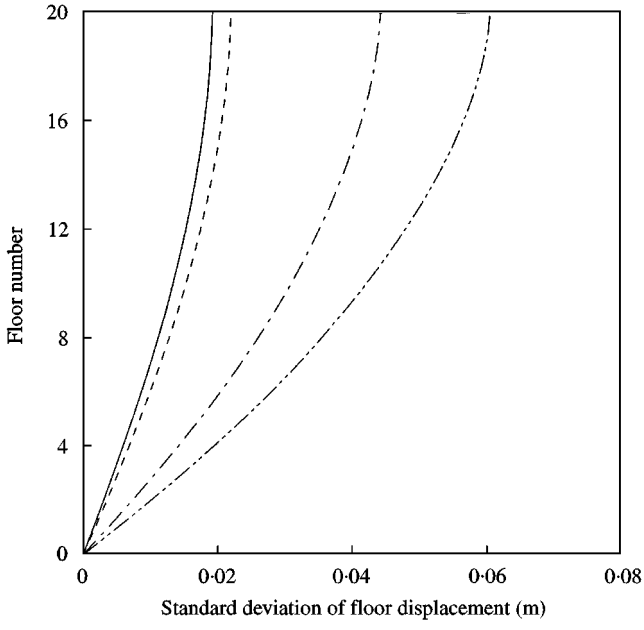

Figure 9. Variations of displacement response of adjacent buildings with height: ——, Left building with damper; – – – –, Right building with damper; — · —, Left building without damper; — · · —, Right building without damper.

the two buildings behave almost as though they are rigidly connected. As a result, the top-floor displacements of the two buildings become the same.

To demonstrate the overall effectiveness of the fluid dampers, the standard deviations of displacement, shear force and acceleration responses at each floor for each building with and without fluid dampers are computed using the Kanai–Tajimi excitation spectrum. Figure 9 shows the variations in the standard deviation of the displacement response relative to the ground with the height of the buildings. The top-floor displacement standard deviation of the unlinked left building is 44·5 mm but with the fluid dampers installed, it is reduced to 19·3 mm, leading to a 57% reduction of the response. For the right building, the top-floor displacement standard deviation is 60·8 mm for the unlinked building and 22·1 mm for the linked building, resulting in a 63% reduction. The reduction of the displacement responses from the fluid dampers is also significant for other floors in either building. The standard deviations of shear force in each story for each buildings are plotted in Figure 10. The shear forces in all the stories of both the buildings are reduced after installation of the fluid dampers. In particular, without the fluid dampers the bottom shear force standard deviation is $1{\cdot}48 \times 10^7$ N in the left building and $1{\cdot}03 \times 10^7$ N in the right building. With the optimum fluid dampers, the base shear force standard deviation is reduced to $6{\cdot}10 \times 10^6$ N in the left building and $3{\cdot}56 \times 10^6$ N in the right building, leading to a 59 and a 65% reduction respectively.

The variations of acceleration response with the building height, as shown in Figure 11, are different from displacement and shear force response profiles shown in Figure 9 and 10. The acceleration response for each unlinked building does not vary monotonically with building height. This is due to the contributions from higher modes of vibration [4]. Clearly, the fluid dampers effectively mitigate the acceleration responses not only from low modes of vibration but also from higher modes of vibration, as indicated by the response curves of the linked adjacent buildings.

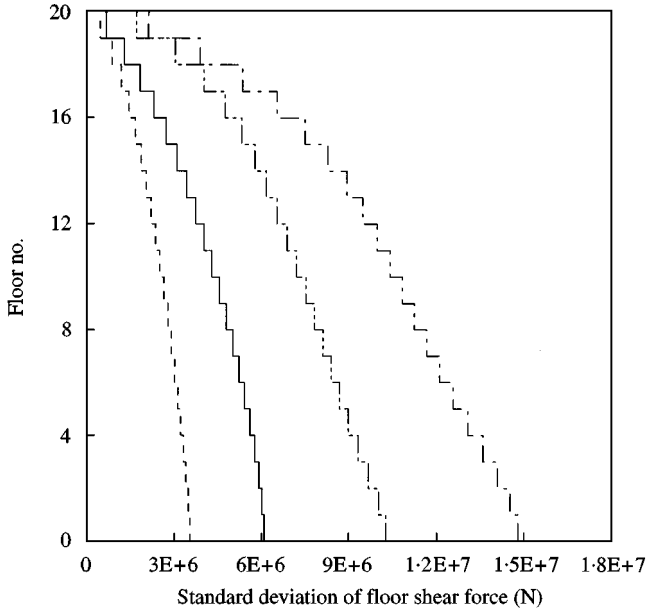

Figure 10. Variations of shear force response of adjacent buildings with height: ——, Left building with damper; – – – –, Right building with damper; — · —, Left building without damper; — · · —, Right building without damper.

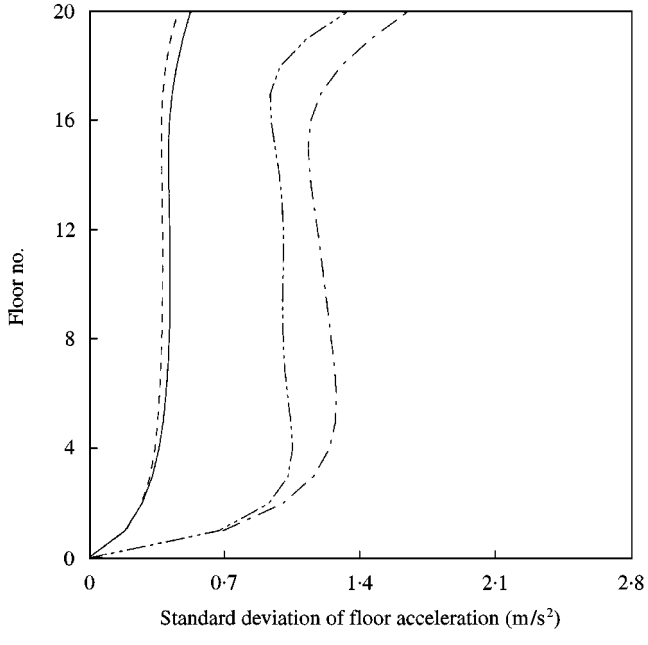

Figure 11. Variations of acceleration response of adjacent buildings with height: ——, Left building with damper; – – – –, Right building with damper; — · —, Left building without damper; — · · —, Right building without damper.

The values of fluid damper forces required for the achievement of significant vibration reduction of the adjacent buildings are important for the design of the fluid dampers and adjacent buildings. In terms of the proposed mixed method, the fluid damper forces can be

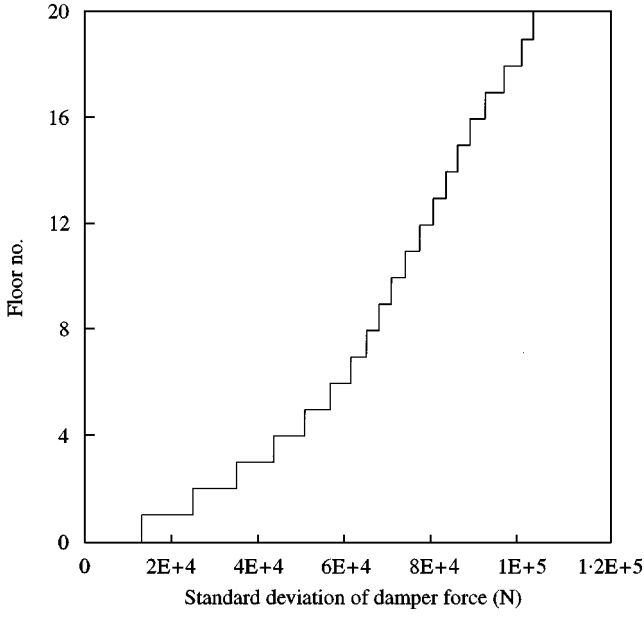

Figure 12. Variations of damper force response of adjacent buildings with height.

easily calculated. The results are shown in Figure 12 for the variations of fluid damper force with the building height. The maximum damper force is about $1{\cdot}0 \times 10^5$ N at the top of the buildings.

It is worthwhile to mention that the maximum reduction levels of seismic responses of the adjacent buildings linked by the Maxwell model-defined fluid dampers are almost the same as those linked by the Voigt model-defined viscoelastic dampers for the given two buildings and the ground motion in the study. This is because in the case of the viscoelastic damper, the required optimal damper stiffness is quite small so that the Voigt model-defined viscoelastic damper is almost a dashpot only. In the case of the fluid damper, the required optimal relaxation time is very small and so the Maxwell model-defined fluid damper also becomes almost a dashpot only. It is also worthwhile to mention that the results obtained in this study are based on the two shear buildings having the same height, mass, and external damping coefficient but different column shear stiffness. For the two buildings with different mass and stiffness ratios and different heights, the effectiveness of the fluid dampers may be different. More information on this aspect can be found in reference [4].

6. CONCLUSIONS

An accurate and effective procedure for determining dynamic characteristics and seismic response of adjacent buildings linked by the Maxwell model defined-fluid dampers has been presented in this paper. The dynamic characteristics of damper-linked adjacent buildings were obtained by solving the eigenvalue problem for real non-symmetric matrices. The random seismic responses of the damper-linked adjacent buildings were determined by a combination of the state-space method and the pseudo-excitation method.

Based on the studies on the example adjacent buildings, it was found that if damper relaxation time and zero-frequency damping coefficient were selected appropriately, the

modal frequencies of the unlinked buildings could be retained and the modal damping ratios of the system could be significantly increased. The earthquake-induced dynamic responses of both buildings could also be tremendously reduced. The optimal values of the dampers found from the modal analysis with the maximum modal damping ratios as an objective were almost the same as those determined from the seismic response analysis with the maximum seismic response as an objective.

When compared with the adjacent buildings linked by the Voigt model-defined viscoelastic dampers, the Maxwell model-defined fluid dampers have the same effectiveness as the viscoelastic dampers under the conditions of the given two buildings ground motion. Some other issues related to this study, such as the optimal position of dampers, the three-dimensional vibration mitigation analysis including torsional effects, and the effect of non-stationary earthquake excitation need a further investigation. The earthquake simulation test to verify the theoretical results is also desirable.

ACKNOWLEDGMENTS

The writers are grateful for the financial support from the Hong Kong Polytechnic University through a HKPU scholarship for the first writer and its Area of Strategic Development Programme in Structural Vibration Control for the second writer. The writers also very much appreciate the help from Mr Craig Winters from Taylor Devices, Inc., U.S.A. in providing us with their sample fluid dampers and useful information.

REFERENCES

1. T. KOBORI, T. YAMADA, Y. TAKENAKE, Y. MAEDA and I. NISHIMURA 1988 *Proceedings of the Ninth World Conference on Earthquake Engineering*, *Tokyo-Kyoto*, *Japan*, Vol V, 773–778. Effect of dynamic tuned connector on reduction of seismic response-application to adjacent office buildings.
2. K. SETO and Y. MATSUMOTO 1996 *Proceedings of the Second International Workshop on Structural Control*, *Hong Kong*, 490–496. A structural vibration control method of flexible buildings in response to large earthquakes and strong winds.
3. Y. YAMADA, N. IKAWA, H. YOKOYAMA and E. TACHIBANA 1994 *Proceedings of the First World Conference on Structural Control*., *Los Angeles*, *CA*, *U.S.A*., Vol. 2, TP2, 41–49. Active control of structures using the joint member with negative stiffness.
4. Y. L. XU, Q. HE and J. M. KO 1999 *Engineering Structures* **21**, 135–148. Dynamic response of damper-connected adjacent buildings under earthquake excitation.
5. M. C. CONSTANTINOU and M. D. SYMANS 1993 *The Structural Design of Tall Buildings*, Vol. 2, 93–132. Experimental study of seismic response of buildings with supplemental fluid dampers.
6. R. B. BIRD, R. C. ARMSTRONG and O. HASSAGER 1987 *Dynamics of Polymeric Liquids*. New York, NY: J. Wiley and Sons.
7. J. H. LIN, W. S. ZHANG and J. J. LI 1994 *Computers and Structures* **50**, 629–633. Structural response to arbitrarily conherent stationary random excitations.